Earthquake Geotechnical Engineering for Protection and Development of Environment and Constructions – Silvestri & Moraci (Eds)
© 2019 Associazione Geotecnica Italiana, Rome, Italy, ISBN 978-0-367-14328-2

A numerical study on the seismic behaviour of cantilever embedded retaining walls in saturated sand

M. Morigi
Università di Roma Tor Vergata, Rome, Italy

R. Conti
Università di Roma Niccolò Cusano, Rome, Italy

G.M.B. Viggiani
University of Cambridge, Cambridge, UK

C. Tamagnini
Università di Perugia, Perugia, Italy

ABSTRACT: Field observations during past earthquakes have shown that quay walls may experience severe damages if positive excess pore water pressures develop in the retained or foundation soil, leading to a reduction of the shear strength and stiffness of the soil or, in extreme cases, to liquefaction. A reliable numerical prediction of seismically induced excess pore water pressures requires the development of a dynamic fully-coupled formulation capable of reproducing solid-fluid interaction together with the adoption of advanced constitutive models. This work presents a numerical study on the dynamic behaviour of cantilever retaining walls embedded in saturated sand. The advanced constitutive model SANISAND, together with an element using a fully-coupled *u-p* dynamic formulation, were implemented in the finite element code FEAP v8.4. The main goal of this work is to investigate the effects of the soil relative density, of the presence of the water table and of the frequency content of the earthquake on the overall seismic response of the wall. The work indicates that different failure mechanisms can develop within the soil-wall system, depending on the amount of excess pore water pressure build-up in the foundation soil. The numerical results are commented with reference to some experimental observations from two small scale dynamic centrifuge tests on a pair of embedded cantilever walls in saturated sand.

1 INTRODUCTION

Field observations collected during past earthquakes indicate that quay walls are particularly vulnerable to strong earthquakes (Iai & Kameota, 1993; Iai, 1998). Water can affect the dynamic behaviour of these structures in at least three different ways: (1) hydrostatic pore water pressures reduce the static effective stress distribution, thus leading to a reduction of stiffness and strength into the soil; (2) it generates additional hydrodynamic pressures on the wall; (3) it can induce further reduction of the effective stress distribution due to pore pressure build up during shaking.

A series of dynamic tests were carried on reduced-scale models of cantilever walls embedded in dry (Conti *et al* 2012; Madabhushi & Zeng, 2006) and saturated (Aversa *et al*., 2015; Madabhushi & Zeng, 2007) sand. These studies revealed significant differences in the response of these systems, depending on the water table position and the relative density of the soil.

This paper presents the main results of a numerical study on the seismic behaviour of cantilever embedded retaining walls, aimed at identifying the role played by the pore water pressure on the overall response of the system. The main objective of the work is to explore the effects

that the relative density of the soil and the different input signals have on the dynamic response of the retaining structure, in terms of displacements and bending moments. The numerical results are commented in the light of the available experimental results.

2 NUMERICAL MODEL

2.1 *Layout of the problem*

Figure 1 shows the layout of the two numerical models considered in this work, consisting of a homogeneous sand layer characterized by different water table conditions: (a) no water table (dry sand) and (b) water table at dredge level (saturated sand). In both cases, a pair of embedded cantilever walls is considered, with a retained height of 4 m and an embedded depth of 5 m. The walls are placed at a distance of 12 m from one another, in order to prevent any interaction during both the static and the dynamic stages.

Two values of relative densities were considered for the soil, representative of an extremely loose (D_r = 12 %) and a medium dense (D_r = 47 %) sand layer, respectively.

Two input signals were used in the analyses, both registered on rock outcrop during the Friuli (Italy) earthquake in 1976 and the Kobe (Japan) earthquake in 1995. Figure 2 shows the acceleration time histories of the two earthquakes, both scaled at a_{max} = 0.2 g, together with the corresponding Fourier amplitude spectra. As shown in the figure, the Friuli and Kobe earthquakes are characterised by a different frequency content, with a dominant frequency of 2.0 Hz and 0.6 Hz, respectively, and strong motion duration, equal to 4.25 s and 12.87 s, respectively. Both factors are relevant for the liquefaction potential of saturated soil deposits.

Focusing the attention on the foundation soil, points A1, P2 and P3 in Figure 1, located 2 m below dredge level and at the soil-wall contact, will be used as reference to discuss the numerical results in terms time history of acceleration (A1) and pore pressure ratio (P2 and P3). Specifically, P2 and P3 are located behind and in front of the wall, respectively.

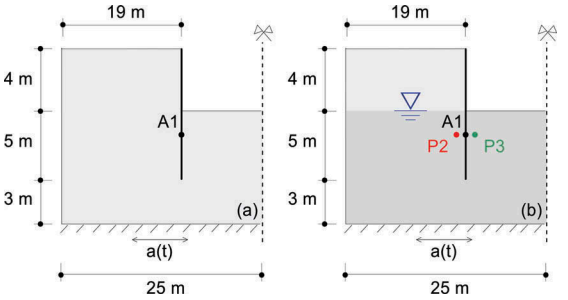

Figure 1. Layout of the problem: (a) dry sand and (b) water table at the dredge level.

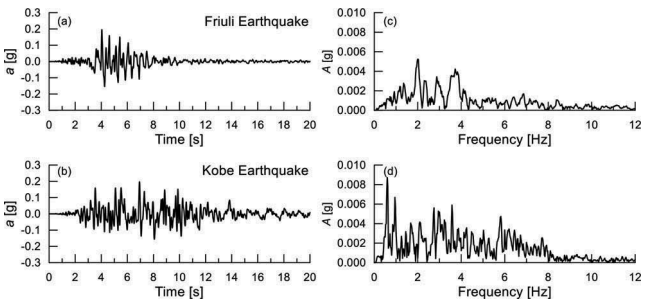

Figure 2. Input signals: (a, c) Friuli and (b, d) Kobe earthquake.

2.2 *Numerical code and constitutive model*

The numerical work presented in this paper was carried out using the finite element code FEAP v8.4 (Taylor, 2013). A 2D plane strain finite element was implemented to solve the dynamic equations of the coupled hydro-mechanical problem, using the *u-p* formulation proposed by Zienkiewicz *et al.* (1980) for a fully saturated porous medium. Both the embedded retaining walls and the soil are modelled with solid elements, using a porous medium formulation for the soil and a non-porous linear-elastic formulation for the walls.

The finite element parameters are the mass density of the soil, ρ_s = 1.85 t/m^3, and of the water, ρ_w = 1.00 t/m^3, the permeability, k = 0.0005 m/s, and the water bulk modulus, K_w = 2.2·10^6 kN/m^2. The constitutive model used for the soil is SANISAND (Dafalias & Manzari, 2004), developed within the framework of critical state soil mechanics and kinematic hardening plasticity, in order to reproduce the main features of the behaviour of sands under cyclic loading. The constitutive equations of the model are briefly recalled in Table 1, together with

Table 1. Summary of the constitutive equations for the SANISAND model

Equation descriptions	Equations	Constants & values
Critical state line	$e_c = e_0 - \lambda_c \left(\frac{p'_c}{p_{at}}\right)^{\xi}$	$e_0 = 0.934$ $\lambda_c = 0.019$ $\xi = 0.7$
Elastic deviatoric strain increment	$d\boldsymbol{e}^e = d\boldsymbol{s}/2G$	-
Small strain shear modulus	$G = G_0 p_{at} \left[\frac{(2.97-e)^2}{(1+e)}\right] \left(\frac{p'}{p_{at}}\right)^{0.5}$	$G_0 = 125$
Elastic volumetric strain increment	$d\in_v^e = dp'/K$	-
Small strain bulk modulus	$K = \frac{2(1+\nu)}{3(1-2\nu)} G$	$\nu = 0.05$
Yield surface	$f = \sqrt{(\boldsymbol{s}-\boldsymbol{\alpha}p') : (\boldsymbol{s}-\boldsymbol{\alpha}p')} - \sqrt{2/3}p'm$ $\boldsymbol{n} = (\boldsymbol{s}/p' - \boldsymbol{\alpha}) / \left(\sqrt{2/3}m\right)$	$m = 0.01$
Plastic deviatoric strain increment	$d\boldsymbol{e}^p = \langle L \rangle \boldsymbol{R}'$	-
Plastic deviatoric strain direction	$\boldsymbol{R}' = B\boldsymbol{n} - C\left(\boldsymbol{n}^2 - 1/3\boldsymbol{I}\right)$ $B = 1 + \frac{3}{2}\frac{(1-c)}{c} g(\theta, c)\cos(3\theta)$ $C = 3\sqrt{\frac{3}{2}}\frac{(1-c)}{c} g(\theta, c)$	- - -
Plastic modulus	$K_p = \frac{2}{3} p' h \left(\boldsymbol{\alpha}_\theta^b - \boldsymbol{\alpha}\right) : \boldsymbol{n}$	-
Boundary surface	$\boldsymbol{\alpha}_\theta^b = \sqrt{2/3}\left[g(\theta, c) M e^{-n^b \psi} - m\right]\boldsymbol{n}$ $h = b_0 / (\boldsymbol{\alpha} - \boldsymbol{\alpha}_{in}) : \boldsymbol{n}$ $b_0 = G_0 h_0 (1 - c_h e) \left(\frac{p_{at}}{p'}\right)^{0.5}$	$M = 1.25$ $c = 0.712$ $n^b = 1.25$ $h_0 = 7.05$ $c_h = 0.968$
Back-stress ratio tensor evolution	$d\boldsymbol{\alpha} = \langle L \rangle (2/3) h \left(\boldsymbol{\alpha}_\theta^b - \boldsymbol{\alpha}\right)$	-
Plastic volumetric strain increment	$de_v^p = \langle L \rangle D$	-
Dilatancy	$D = A_d \left(\boldsymbol{\alpha}_\theta^d - \boldsymbol{\alpha}\right) : n$	-
Dilatancy surface	$\alpha_\theta^d = \sqrt{2/3}\left[g(\theta, c) M e^{n^d \psi} - m\right]\boldsymbol{n}$ $A_d = A_0 \left(1 + \sqrt{3/2}\langle \boldsymbol{z} : \boldsymbol{n} \rangle\right)$	$n^d = 2.1$ $A_0 = 0.704$
Fabric-dilatancy tensor evolution	$d\boldsymbol{z} = -c_z \langle -de_v^p \rangle \left(\sqrt{2/3} z_{max} \boldsymbol{n} + \boldsymbol{z}\right)$	$c_z = 600$ $z_{max} = 2$

the numerical values adopted for the parameters, while details of the implementation are given in Morigi *et al.* (2018).

The physical and mechanical parameters of the walls are: mass density, $\rho = 2.40$ t/m^3, Young's modulus, $E = 30$ GPa and Poisson's ratio, $\nu = 0.2$. The thickness of the walls is 0.5 m. There is no interface between the retaining walls and the soil.

2.3 *Procedure of analysis*

During the static stage, standard boundary conditions were applied to the model. After the geostatic stress state was imposed, the excavation was carried out removing the soil elements between the walls in 8 successive steps.

During the dynamic stage, periodic constraints were applied to the lateral boundaries of the mesh, both for the mechanical and the hydraulic problem, and the selected acceleration–time histories were applied to the bottom nodes of the grid in the horizontal direction (rigid boundary).

3 RESULTS

3.1 *Model A: Cantilever walls in dry sand*

Figure 3 shows the main results for the case of cantilever walls embedded in a homogeneous layer of medium dense dry sand ($D_r = 47$ %). Specifically, Figure 3 shows, for the left wall: (a) the distribution of horizontal effective contact stresses, together with the theoretical static distribution provided by Lancellotta (2002) for $\phi = 31°$ and $\phi = \phi/3$; (b) the horizontal relative displacements; (c) the bending moment distribution in the wall; (d, e) the acceleration time histories of the input signals and those computed at the reference point A1. The results for

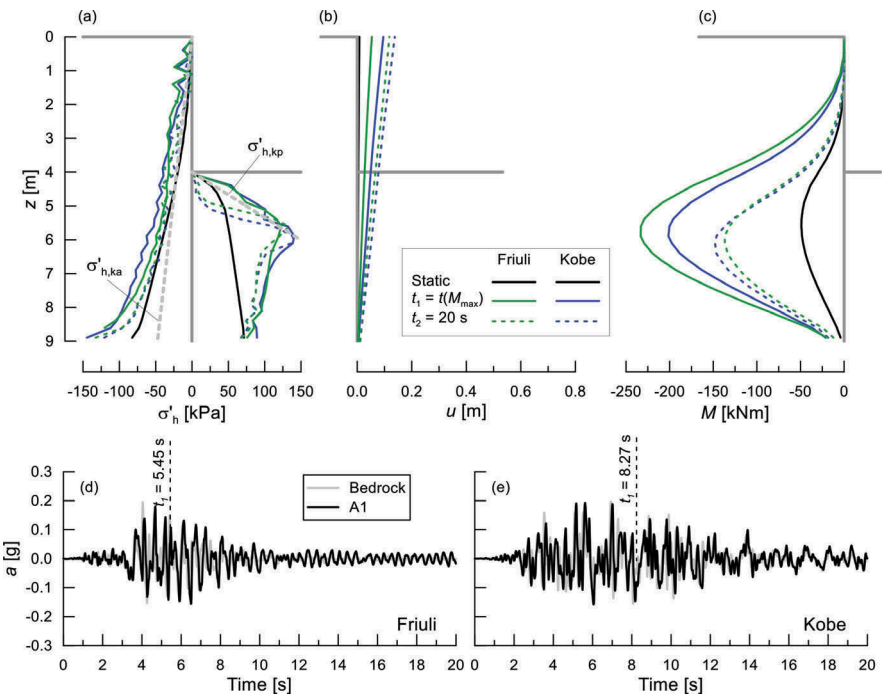

Figure 3. Dry medium-dense sand: (a) horizontal contact stresses; (b) relative displacement of the wall; (c) bending moment; (d, e) accelerations time histories.

both Friuli and Kobe earthquake are shown. Moreover, the distributions refer to the static stage (black lines) and to two relevant time instants, i.e.: t_1, corresponding to which the bending moment reaches its maximum value (continuous lines); and t_2, approximately at the end of the earthquake (dashed lines).

During the earthquake, inertia forces into the soil induce an increase of the horizontal stresses behind the wall. Consequently, the progressive rotation of the wall leads to a mobilization of the soil passive strength in front of the wall and to an increase of bending moment. Maximum and residual bending moments correspond to about 480 % and 310 % (Friuli earthquake) and 410 % and 300 % (Kobe earthquake) of the static value, respectively. Both maximum and residual bending moments are very close to each other, irrespective of the applied earthquake, thus suggesting that, in this case, the maximum internal forces are related to the strength of the system rather than the characteristics of the input signal.

The acceleration time histories computed at point A1 are very similar to the input ones, indicating that no significant amplification phenomena occurred up to dredge level. This evidence is related to the short distance between the reference point A1 and the bottom of the mesh (6 m). Accelerations are amplified, instead, close to the soil surface, where amplification ratios of 2.7 (Friuli) and 3.4 (Kobe) were computed between the maximum wall acceleration and the input one.

Figure 4 shows the same results for the case of cantilever walls embedded in a homogeneous layer of extremely loose dry sand (D_r = 12 %). The wall exhibits approximately the same behaviour observed in the previous case. As a matter of fact, inertia forces into the soil lead to a progressive increase of contact stresses, wall displacements and internal forces. Moreover, the computed maximum and residual bending moments are similar to the previous case, indicating a minor effect of the soil relative density. On the other hand, D_r has a clear effect on the horizontal displacements of the wall. In this case, in fact, an increase of about 120% can be observed with respect to the medium dense case. Again, the computed horizontal

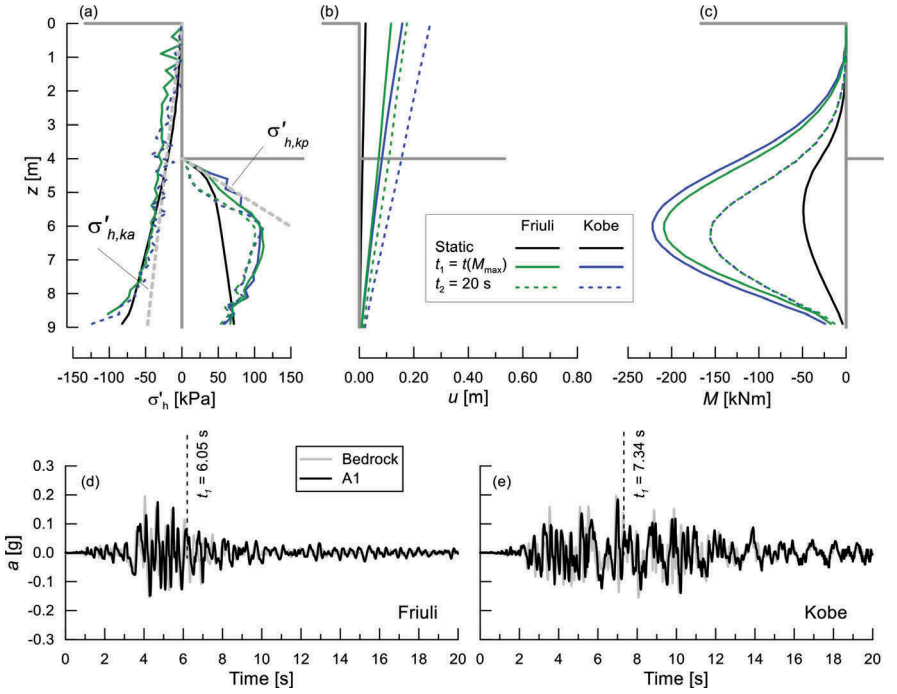

Figure 4. Dry loose sand: (a) horizontal contact stresses; (b) relative displacement of the wall; (c) bending moment; (d, e) accelerations time histories.

accelerations (Figure 4d,e) do not show significant amplification phenomena into the sand layer, at least up to the reference point A1.

3.2 *Model B: cantilever walls in saturated sand*

Figure 5 shows the main results for the case of cantilever walls embedded in a homogeneous layer of medium dense sand (D_r = 47 %), in which the water table is located at dredge level. Results are shown in the same format as for the previous cases. Figure 5(d,e) show also the time histories of the normalised pore pressure ratio $r_u = \Delta_u/\sigma'_{v0}$ computed at the reference points P2 and P3.

This time, the soil-wall system exhibits a different behaviour with respect to what observed in the dry sand models. Inertia forces in the soil induce again a redistribution of the effective horizontal stresses at the soil-wall contact, with an increase of the maximum bending moment of about 180 % (Kobe) and 120 % (Friuli) of the corresponding static value, while the residual bending moments are close to the static one. It is worth noting that internal forces in the wall are related to total stresses, thus including the effect of the pore water pressure distribution, which is not shown in the figure. This time, the maximum internal forces in the wall show a certain dependence on the characteristics of the applied signal.

A better understanding of the results outlined above is provided by the time histories of the accelerations (A1) and the r_u ratios (P2 and P3) in Figure 5(d,e). Behind the wall (P2), r_u increases progressively during the strong motion stage, reaching a value of about 0.5 under both earthquakes. In front of the wall (P3), instead, pore-pressures evolve differently during the applied signals. Specifically, the significant oscillations computed during the Kobe earthquake, with r_u reaching also negative values (Figure 5e), are clearly related to the dilatant behaviour of the soil below dredge level, where the mean effective stress is small. The different behaviour induced by the two earthquakes was similarly observed by Morigi et al. (2018) in 1D site response analyses and is strictly related to the different frequency content of the two signals. Overall, the pore pressure build-up leads to a reduction of the state of effective stress but, as suggested by the acceleration time histories computed at point A1, the soil does not fully liquefy.

Looking at the final horizontal displacements (Figure 5b), the rotation of wall occurs together with a translation of the tip, clearly related to a temporary reduction of the available

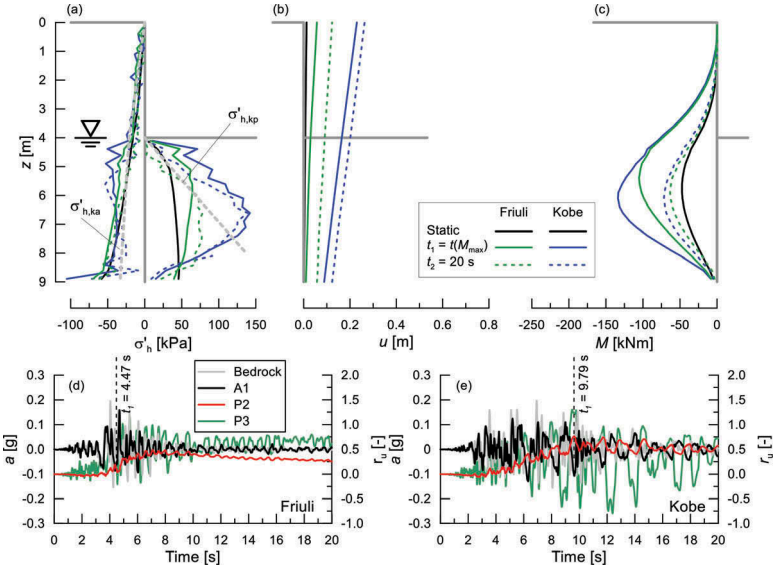

Figure 5. Saturated medium-dense sand: (a) horizontal contact stresses; (b) relative displacement of the wall; (c) bending moment; (d, e) accelerations and r_u time histories.

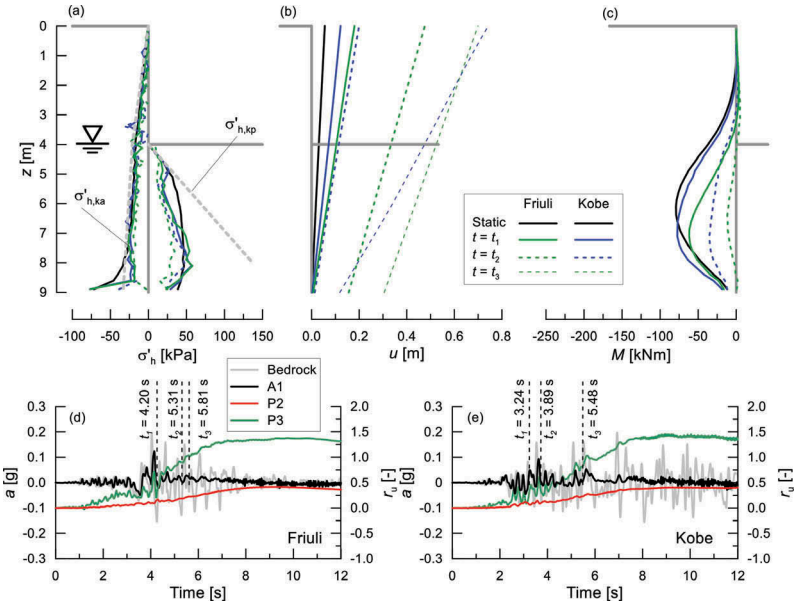

Figure 6. Saturated loose sand: (a) horizontal contact stresses; (b) relative displacement of the wall; (c) bending moment; (d, e) accelerations and r_u time histories.

shear strength in the foundation soil. This observation is also consistent with a partial liquefaction of the saturated sand below dredge level.

Figure 6 shows the results for the case of cantilever walls embedded in a homogeneous layer of extremely loose saturated sand (D_r = 12 %), with the water table located at dredge level. This time, liquefaction occurs in front of the wall during both the applied earthquakes, as indicated by the time histories of r_u (P3), which remain close to one during the whole duration of the strong motion (values of $r_u > 1$ are possible in 2D conditions). As a result, the liquefied soil cannot propagate shear stresses and the horizontal accelerations computed at point A1 are damped. In this case, the attenuation does not depend on the frequency content of the earthquake.

The complete loss of strength in the foundation soil leads to a collapse of the walls. Accordingly, the dynamic distributions of contact horizontal effective stresses, horizontal displacements and bending moment in the wall are shown only for three time instants during the strong motion stage, *i.e.* before excessive wall displacements took place.

The horizontal effective stress profiles show a progressive reduction, compared with the static distribution, implying also a consistent reduction of the bending moment distribution. In other words, the applied earthquakes do not induce an increment of internal forces in the wall, as liquefaction inhibits the propagation of substantial inertia forces into the soil. On the other hand, the collapse of the wall is related to the accumulation of excessive permanent displacements.

4 COMPARISON OF NUMERICAL RESULTS WITH EXPERIMENTAL DATA

The layout of the numerical models discussed in this paper is similar to some of the reduced scale centrifuge models presented in the recent literature, referring to a couple of cantilever walls embedded in a homogeneous layer of dry (Conti *et al.,* 2012) and saturated (Aversa *et al.*, 2015) sand, reconstituted at different values of the soil relative density.

Although the geometry of the models is slightly different and the constitutive parameters adopted for the SANISAND model were not calibrated to reproduce the cyclic behaviour of the Leighton Buzzard sand used in the centrifuge tests, numerical and experimental results share some common features, as detailed below:

i. for cantilever walls embedded in dry sand, the relative density of the soil has minor effects on the maximum internal forces, while it affects substantially the final horizontal displacements;
ii. in the case of saturated sand, the relative density of the soil plays a crucial role, as the occurrence of liquefaction phenomena in the foundation soil is directly related to D_r. Moreover, in this case, the seismic performance of the wall should be evaluated with reference to the final permanent displacements rather than to the maximum internal forces.
iii. if high excess pore water pressures develop within the foundation soil, the rotation of wall is associated with a substantial displacement of the tip.

5 CONCLUSIONS

This paper presented the results of a numerical study on the seismic behaviour of cantilever retaining walls embedded in a homogeneous layer of dry and saturated sand. Two values were adopted for the soil relative density, representative of a medium dense and a loose sand layer, respectively, and two dynamic inputs were applied to the models, characterised by different frequency contents and strong motion durations.

As far as the dry sand models are concerned, the analyses showed that maximum internal forces in the wall depend on the strength of the system, rather than the characteristics of the applied earthquake. Moreover, the soil relative density has a negligible effect on the maximum bending moment while is affects the final permanent displacement.

For the saturated case, D_r is the crucial parameter for the evaluation of the seismic stability of the system, as it determines the occurrence of liquefaction phenomena within the foundation soil. The numerical analyses showed that liquefaction occurs only for a short time interval in the medium dense sand case, while it lasted for the whole duration of the strong motion stage, eventually leading to the collapse of the wall.

REFERENCES

Aversa S., de Sanctis L., Maiorano R.M.S., Tricarico M., Viggiani G., Conti R., Madabhushi G.S.B. 2015. Centrifuge Modelling of Retaining Walls Embedded in Saturated Sand Under Seismic Actions. In Taucer F., Apostolska R. (eds.), Experimental Research in Earthquake Engineering. Geotechnical, Geological and Earthquake Engineering 35. Cham: Springer.

Conti, R., Madabhushi, G.S.P., & Viggiani, G.M.B. 2012. On the behaviour of flexible retaining walls under seismic actions. *Géotechnique*, 62(12): 1081-1094.

Dafalias, Y.F. & Manzari M.T. 2004. Simple plasticity sand model accounting for fabric change effects. *Journal of Engineering Mechanics*, 130(6): 622–634.

Iai S. 1998, Rigid and Flexible Retaining Walls During Kobe Earthquake. In *International Conference on Case Histories in Geotechnical Engineering*, St. Louis, Missouri, March 8, 1998.

Iai, S. & Kameoka T. 1993. Finite element analysis of earthquake induced damage to anchored sheet pile quay walls. *Soil and Foundations*, 33(1): 71–91.

Lancellotta R. 2002. Analytical solution of passive earth pressure *Géotechnique* 52(8): 617–619.

Madabhushi G.S.P. & Zeng X. 2006. Seismic response of flexible cantilever retaining walls with dry
Backfill. *Geomechanics and Geoengineering: An International Journal*, 1(4): 275–289.

Madabhushi G.S.P. & Zeng X. 2007. Simulating Seismic Response of Cantilever Retaining Walls. *Journal of Geotechnical and Geoenvironmental Engineering*, 133(5): 539–549.

Morigi, M., Viggiani, G.M.B., Conti, R., Tamagnini, C. 2018. Numerical simulation on the ground response in saturated sand. In Cardoso, A.S., Borges, J.L., Costa, P.A., Gomes, A.T., Marques, J.C., Vieira, C.S. (eds.), *Numerical Methods in Geotechnical Engineering IX*, Volume 2. Porto June 25–27, 2018. London: CRC Press.

Taiebat, M, Jeremic, B., Dafalias, Y.F., Kaynia A.M., Cheng Z. 2010. Propagation of seismic waves through liquefied soils. *Soil Dyn. Earthquake. Eng*., 30: 236–257.

Taylor, R.L. 2013. *Feap - a finite element analysis program - version 8.4 User manual*. Technical report, Berkeley: University of California at Berkeley.

Zienkiewicz, O.C., Chang C.T., Bettess P. 1980. Drained, undrained, consolidating and dynamic behaviour assumptions in soils. *Géotechnique*, 30(4): 385–395.